UCRL- 97898
PREPRINT

PELLET ABLATION MODELING IN REACTOR-GRADE PLASMAS WITH FUSION-BORN ALPHA PARTICLES

S. K. Ho
L. J. Perkins

This paper is prepared for submittal to
Fusion Technology

December 18, 1987

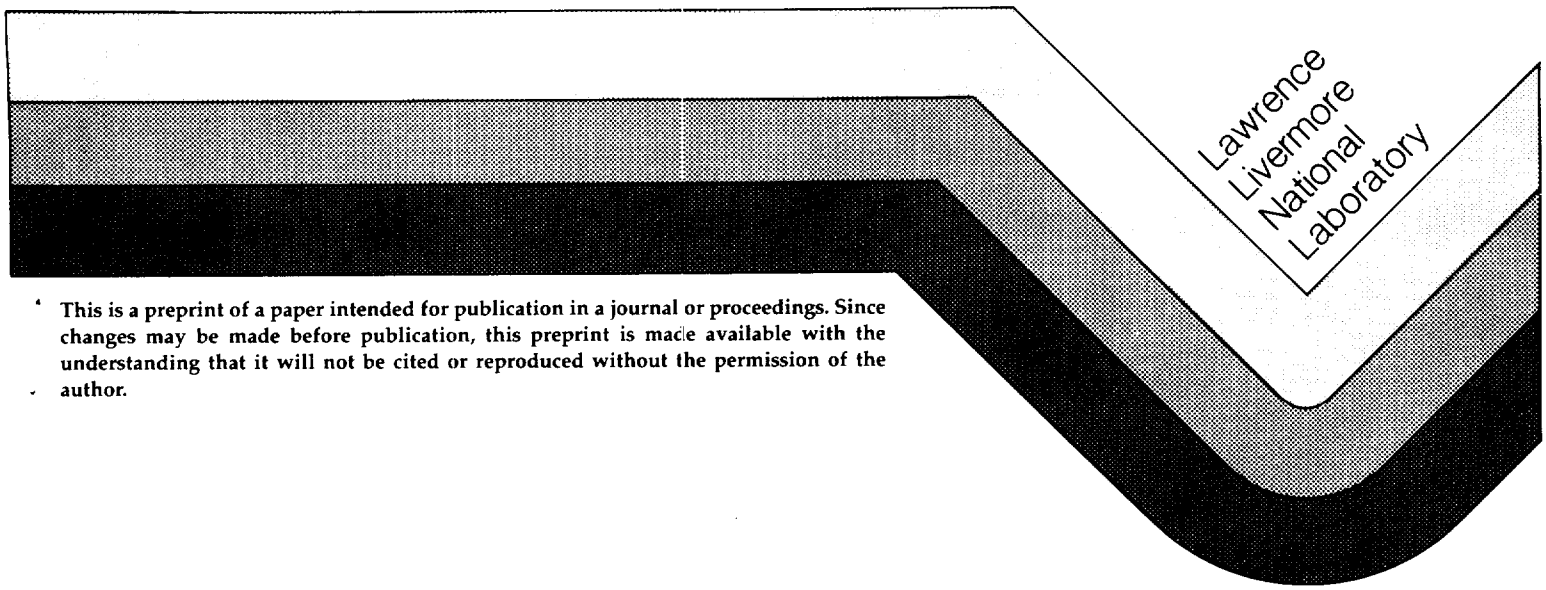

DISCLAIMER

PELLET ABLATION MODELING IN REACTOR-GRADE PLASMAS WITH FUSION-BORN ALPHA PARTICLES *

S. K. Ho and L. J. Perkins
Lawrence Livermore National Laboratory
University of California
P.O. Box 5511, L-644
Livermore, CA 94550
(415) 423-6012

December 18, 1987

Total number of pages 24
Total number of tables 1
Total number of figures 7

*This work was performed under the auspices of the U.S. Department of Energy by Lawrence Livermore National Laboratory under contract No. W-7405-Eng-48.

PELLET ABLATION MODELING IN REACTOR-GRADE PLASMAS WITH FUSION-BORN ALPHA PARTICLES

ABSTRACT

The modeling of fuel pellet ablation is performed for two ablating species: plasma electrons and fusion-born alpha particles. A transonic flow, neutral shielding model is adapted and the electrons and alphas are modeled in the monoenergetic representation. Numerical solutions of the eigenvalue equations describing both the shielding cloud hydrodynamics and the energy degradation of the ablating species, enable the formulation of simple scaling laws for the pellet ablation rate due to the combined effect of electrons and alphas. For the TIBER II Engineering Test Reactor design, a moderate alpha enhancement of about 5% of the electron ablation rate is calculated.

I. Introduction

Pellet Injection has received much attention for tokamak fueling due to the attractiveness of depositing fuel inside the plasma relative to edge gas puffing.[1,2] Following the idea of injecting frozen deuterium-tritium (DT) pellets for plasma fueling, originally suggested by Spitzer and Tonks,[3] various pellet ablation models[4-13] have been proposed to predict the pellet lifetime inside the plasma. The difference in the models is mainly in the pellet shielding mechanisms and the dynamics of the ablated materials. These shielding mechanisms have included electrostatic, cold plasma, neutral gas and magnetic field distortion.

The neutral shielding model[7-9] so far has shown good agreement with past pellet injection experiments,[1-2] which operated at a low plasma temperature and density relative to that expected for a fusion reactor. The model proposes that the molecules are ablated from the pellet as neutral particles. The resulting neutral cloud surrounding the pellet then undergoes an expansion away from the pellet. This neutral cloud interacts with the incident plasma electrons and effectively reduces the energy flux that vaporizes the pellet.

Recent improvements[13] of the neutral shielding model suggests the inclusion of a cold plasma blanket outside the neutral cloud that absorbs part of the incoming energy flux before entering the cloud.

The electrons provide the dominant heat flux because they have a much larger speed than that of the ions in a plasma with comparable electron and ion temperatures. As a consequence, most pellet ablation calculations are based on electron ablation alone. The effects of including the fast ions from neutral beam injection have been examined by Milora and Nakamura et al., following the approaches of Refs. 9 and 8, respectively. However, there is no general formulation of the results for further applications of modeling two ablating species.

In this work, we examine pellet ablation in a reactor-grade plasma in which, in addition to the plasma electrons, fusion-born alpha particles may also contribute to the pellet ablation. The low alpha density is partially compensated by the high alpha energy, which makes the alpha heat flux an appreciable fraction of that of the electron heat flux. Thus, the pellet ablation calculations become a two ablating species problem with comparable energy fluxes. The objective of our work is to assess the effects of fast alphas in pellet ablation and modify the pellet ablation scaling law accordingly.

It should be mentioned that we will adopt the neutral shielding model by Parks and Turnbull[8] for our work. The validity of the neutral shielding model, as with all pellet ablation models, has not yet been experimentally verified in a reactor-grade plasma. Their model is used because of the formal simplicity of the set of coupled hydrodynamic equations employed and the good agreement with pellet injection experiments in lower temperature and density plasmas. Thus, results of the effect of alpha ablation obtained should be interpreted as consistent within the context of the neutral shielding model. Future refinements could include the effects of cold plasma shielding.[13]

II. Energy Flux Attenuation

One of the main objectives in pellet ablation calculations is to determine the degradation of the incident energy flux based on the shielding model assumed. The lifetime of the pellet is directly related to the incident

energy flux and the effectiveness of its attenuation. The energy flux attenuation calculations involve solving a coupled set of hydrodynamic equations describing the shielding cloud and incoming particles self-consistently. In this section, we will describe the equations for the attenuation of energy and energy flux of the electrons and alpha particles. A comparison of the penetration range of the two species will also be made for better understanding of their roles in pellet ablation. This will be discussed in more details in Section IV.

Incident plasma electrons and fusion-born alpha particles passing through the neutral shielding cloud will undergo inelastic processes such as excitation and ionization of the neutral atoms and molecules, and elastic scattering with the neutrals. As a result, the particles lose energy as they travel inside the neutral cloud. The energy loss for particles which travel along the magnetic field inside an ablation cloud can be related by

$$\frac{dE(r)}{dr} = \frac{n(r)\ L(E)}{\langle \cos\theta \rangle} \tag{1}$$

where dE/dr is the reduction of particle energy per unit length, n(r) is the local number density of the ablatant neutral particles, L(E) is the energy dependent energy loss function of the incident particles, and $\langle \cos\theta \rangle$ is the average pitch angle of the particles with respect to the magnetic field. For an isotropic distribution of the incident particles, the $\langle \cos\theta \rangle$ term is approximated by 1/2. The energy flux of the particles, q, can be formulated in a similar fashion:

$$\frac{d\ q(r)}{dr} = n(r)\ \Lambda(E)\ q(r) \tag{2}$$

with $\Lambda(E)$ being an effective flux attenuation cross-section.

For the plasma electrons, if we approximate the Maxwellian distribution by an equivalent monoenergetic distribution characterized by energy flux q_{eo} and energy E_{eo}, then q_{eo} and E_{eo} are related to the plasma electron temperature T_{eo} and density n_{eo} by

$$q_{eo} = \frac{n_{eo}\ v_{eo}\ E_{eo}}{4} \tag{3}$$

and $E_{eo} = 2\ k\ T_{eo}$ (4)

where $v_{eo} = (8\ k\ T_{eo}/\pi\ m_e)^{1/2}$ and k is the Boltzmann constant. As for the fusion-born alphas, we assume a steady-state slowing down distribution of the form

$$f_\alpha(v) = \frac{S\ \tau_s}{4\ \pi\ (v^3 + v_c^3)} \tag{5}$$

where S is the fusion alpha birth rate, τ_s is the slowing down time, and v_c is the critical velocity. For a plasma composed of a 50/50 mix of D and T, they can be expressed as,

$$S = n_e^2\ \langle\sigma v\rangle/4$$

$$\tau_s = \frac{3\ m_\alpha\ T_e^{3/2}}{16\ \sqrt{2\pi m_e}\ e^4\ \ell n\Lambda\ n_e}$$

$$v_c = \left(\frac{5\sqrt{\pi}}{4}\ \frac{m_e}{m_\alpha}\right)^{1/3} v_e$$

Then the alpha number density can be found by integrating Eq. (5) in velocity space to obtain

$$n_{\alpha o} = \frac{S\ \tau_s}{3}\ \ell n\ \left(\frac{v_\alpha^3 + v_c^3}{v_c^3}\right) \tag{6}$$

We also approximate the alpha distribution in the form of Eq. (5) as monoenergetic by computing a representative mean energy $E_{\alpha o}$ for the alphas with density $n_{\alpha o}$. We follow the approach of Ref. 16 in weighting slightly favorably with velocity, i.e.,

$$E_{\alpha o}^3 = \int \left(\tfrac{1}{2}\ m\ v^2\right)^3\ f_\alpha\ d^3v$$

This results in a mean alpha energy given by

$$E_{\alpha o} = 1/2\ m v_\alpha^2 \left\{ \frac{1/2 - \frac{v_c^3}{v_\alpha^3}}{\ell n\ (1 + \frac{v_\alpha^3}{v_c^3})} - \frac{v_c^6}{v_\alpha^6} \right\}^{1/3} \tag{7}$$

For typical reactor-grade plasmas, $E_{\alpha o}$ is in the range of 1.7 to 2.0 MeV.

In order to define the effective flux attenuation cross-section, the energy flux for a monoenergetic incident beam of particles can be written:

$$q(r) = q_o \frac{E(r)}{E_o} \exp\ (-\int_{E(r)}^{E_o} \frac{\sigma_T(E)}{2L(E)}\ dE) \tag{8}$$

where σ_T is the effective backscattering cross-section. The flux is degraded by both the energy loss through L(E) and the particle loss from $\sigma_T(E)$. Hence, by combining Eqs. (2) and (8), we may define the effective flux attenuation cross-section as in Refs. 7 and 8

$$\Lambda(E) = \sigma_T(E) + 2\ L(E)/E \tag{9}$$

Equations (1) and (2) will be used in conjunction with the hydrodynamic equations which solve n(r) self-consistently.

Next, we find the appropriate expressions of L(E) and $\sigma_T(E)$ for both the electrons and alphas in the energy range of interest for our problem. The electron energy loss function in molecular hydrogen has been studied by Miles et al.[17] A semi-empirical formula is fitted

$$L_e(E) = 8.62 \times 10^{-15}\ [(\frac{E}{100})^{0.823} + (\frac{E}{60})^{-0.124} + (\frac{E}{48})^{-1.94}]^{-1} \text{eV-cm}^2 \tag{10}$$

where E is in unit of eV. We take the form of σ_T from Refs. 7 and 8, which adjusted the elastic scattering cross-section for electrons or atomic hydrogen based on the Born approximation to reflect the experimentally determined values, and is given by

$$\sigma_T(E) = \begin{cases} \dfrac{8.8 \times 10^{-13}}{E^{1.71}} - \dfrac{1.62 \times 10^{-12}}{E^{1.932}} & E > 100 \text{ eV} \\ \dfrac{1.1 \times 10^{-14}}{E} & E < 100 \text{ eV} \end{cases}$$

The alpha energy loss function in hydrogen has been tabulated from scaling with experimentally determined data in Ref. 18. We perform a polynomial fit of the tabulated data and obtain an expression for L_α as

$$L_\alpha(E) = 2.14 \times 10^{-15} \left\{1 + 2.312 \left(\frac{E}{10^5}\right) - 0.165 \left(\frac{E}{10^5}\right)^2 + 4.267 \times 10^{-3} \left(\frac{E}{10^5}\right)^3 - 3.737 \times 10^{-5} \left(\frac{E}{10^5}\right)^4 \right\} \text{ eV-cm}^2 \qquad (12)$$

where E is also in units of eV. Since the alphas suffer much less scattering as compared with the electrons, the depletion of alpha energy is dominated by the drag energy loss while that due to scattering is negligible. Hence, for simplicity, we assume that $\sigma_{T\alpha}$ is zero.

At this point, it is instructive to compare the penetration range of the electrons and alphas as a function of their energies. Table 1 shows the range of electrons and alphas stopping in a STP hydrogen molecular gas at their respective energy range of interest. The results are obtained by integrating Eq. (1) with L_e and L_α given by Eqs. (10) and (12), respectively. Note that the calculations are performed for monoenergetic beams of electrons and alphas, and the electron energy is shown in terms of the plasma electron temperature through Eq. (4). We may recall from our alpha energy and flux modeling that the alpha energy is about 1.7 to 2.0 MeV in the monoenergetic representation. Hence, we see that the alphas have a longer penetration distance if the plasma electron temperature is less than about 10 keV. This observation can be applied to our pellet ablation modeling in that the alpha ablation dominates if the electron temperature is less than 10 keV because the ablated cloud thickness is determined from the condition to shield the alphas from penetrating to the pellet surface. The situation is reversed if the electron temperature is greater than about 10 keV. Therefore, from this simple comparison, we expect the alpha contribution to pellet ablation to be

TABLE 1 Penetration range of monoenergetic electrons and alphas in STP hydrogen molecules.

Electrons		Alpha Particles	
T_e (keV)	R_e (cm)	E_α (MeV)	R_α (cm)
6	1.49	1.0	2.92
8	2.51	1.5	3.68
10	3.75	2.0	4.53
12	5.22	2.5	5.56
14	6.91	3.0	6.78
16	8.80	3.5	8.10

very small if the average plasma electron temperature is much higher than 10 keV.

III. Formulation of Equations

The formulation of the governing hydrodynamic equations for the ablation cloud coupling with the energy flux degradation equations for the two ablating species (electrons and alphas) is an extension of the single ablating species model by Parks and Turnbull.[8] This has been similarly adapted for high energy neutral beam ions in Ref. 15.

The dynamics of the ablation cloud are governed by the basic conservation equations in mass, momentum, and energy, plus an equation of state. For an ideal gas with constant specific heat expanding with spherical symmetry in the radial direction r, the equations can be written as:

$$\rho v r^2 = \frac{G}{4\pi} \tag{13}$$

$$\rho v \frac{dv}{dr} + \frac{dp}{dr} = 0 \tag{14}$$

$$\frac{G}{4\pi^2} \frac{d}{dr} \left(\frac{\gamma\, kT}{(\gamma-1)m} + \frac{v^2}{2}\right) = f_e \frac{dq_e}{dr} + f_\alpha \frac{dq_\alpha}{dr} \tag{15}$$

where ρ, v, T, p are the local values of mass density, expanding velocity, temperature and pressure of the ablation cloud, respectively; m is the mass of a pellet molecule, γ is the ratio of specific heat, and G is the ablation rate. Two factors f_e and f_α are used to specify the fraction of electron and alpha energy flux losses that are available to heat the ablation cloud. We assume the conventionally used values[8] of $f_e = 0.65$ and $f_q = 1.0$ which account for small gyroradius of the electrons and larger finite gyroradius for the alphas.

The energy and energy flux degradation equations are rewritten explicitly with the local dynamic variables for the two ablating species:

$$\frac{dq_e}{dr} = \frac{\rho \Lambda_e\, q_e}{m} \tag{16}$$

$$\frac{dE_e}{dr} = \frac{2\rho L_e}{m} \tag{17}$$

$$\frac{dq_\alpha}{dr} = \frac{\rho \Lambda_\alpha q_\alpha}{m} \tag{18}$$

$$\frac{dE_\alpha}{dr} = \frac{2\rho L_\alpha}{m} \tag{19}$$

The appropriate boundary conditions are evaluated at the pellet surface $r = r_p$, and the plasma conditions without the influence of the pellet are evaluated at $r \to \infty$. The boundary condition at the pellet surface can be easily understood from the view that the basic function of the ablation cloud is to absorb the incident energy flux so that the pellet will not be evaporated instantaneously upon exposure to the incoming flux. The energy flux reaching the pellet surface is negligible compared with the unattenuated flux and is approximately zero. If the energy flux is completely absorbed far from the pellet surface or a significant amount of flux remains at the pellet surface, the ablation rate will change to adjust the ablation cloud thickness accordingly so that the energy flux vanishes at the pellet surface. Moreover, minimal energy is delivered at the pellet surface so that the ablated molecules do not evaporate with any appreciable kinetic energy. The other boundary conditions at $r \to \infty$ are simply that the electrons and alphas retain their unattenuated incident energies and energy fluxes. In terms of our variables, the boundary conditions are:

$$q_e (r_p) + q_\alpha (r_p) = 0 \tag{20}$$

$$V (r_p) = 0 \tag{21}$$

$$q_e (\infty) = q_{eo} \tag{22a}$$

$$E_e (\infty) = E_{eo} \tag{22b}$$

$$q_\alpha (\infty) = q_{\alpha o} \tag{22c}$$

$$E_\alpha (\infty) = E_{\alpha o} \tag{22d}$$

The set of equations (13) to (19) with the boundary conditions (20) to (22) completely defines the pellet ablations process. We briefly outline the

approach and algorithm of solving this set of equations in the remainder of this section. As introduced by Ref. 8, since the expansion flow is transonic, it is convenient to normalize the variables in terms of their values at the sonic radius where the expanding cloud has a Mach number of unity. The new variables are defined by:

$$r' = \frac{r}{r_*}$$

$$T' = \frac{T}{T_*}$$

$$\rho' = \frac{\rho}{\rho_*}$$

$$w' = \frac{v^2}{v_*^2}$$

$$q_j' = \frac{q_j}{q_{j_*}}$$

$$E_j' = \frac{E_j}{E_{j_*}}$$

where the quantities with an asterisk subscript are evaluated at the sonic radius and subscript j denotes either e or α.

In the new variables system, Eq. (13) is used to eliminate ρ', and Eqs. (14) to (19) are then transferred to a set of coupled first order ODE:

$$\frac{dw'}{dr'} = \frac{4\, w'\, T'}{r'\,(T' - w')}\left(\frac{Q\, r'}{\sqrt{w'}\, T'} - 1\right) \tag{23}$$

$$\frac{dT'}{dr'} = \left(\frac{2Q}{\sqrt{w'}}\right) - \frac{(\gamma - 1)}{2}\frac{dw'}{dr'} \tag{24}$$

$$\frac{dE_e'}{dr'} = \frac{2\,\lambda_*\, L_e}{\sqrt{w'}\, r'^2\, \Lambda_{e_*}\, E_{e_*}} \tag{25}$$

$$\frac{dq_e'}{dr'} = \frac{\lambda_* \Lambda_e q_e'}{\sqrt{w'} r'^2 \Lambda_{e_*}} \tag{26}$$

$$\frac{dE_\alpha'}{dr'} = \frac{2\lambda_* L_\alpha}{\sqrt{w'} r'^2 \Lambda_{e_*} E_{\alpha_*}} \tag{27}$$

$$\frac{dq_\alpha'}{dr'} = \frac{\lambda_* \Lambda_\alpha q_\alpha'}{\sqrt{w'} r'^2 \Lambda_{e_*}} \tag{28}$$

where we have defined an effective energy flux Q and an eigenvalue of the problem λ_* as,

$$Q = \frac{f_e q_{e_*} \Lambda_e q_e' + f_\alpha q_{\alpha_*} \Lambda_\alpha q_\alpha'}{f_e q_{e_*} \Lambda_{e_*} + f_\alpha q_{\alpha_*} \Lambda_{\alpha_*}} \tag{29}$$

$$\lambda_* = \frac{\rho_* r_* \Lambda_{e*}}{m} \tag{30}$$

Note that the energy loss function L and effective flux attenuation cross-section Λ for the electrons and alphas are not normalized.

In deriving Eqs. (23) to (28), we have used the criterion that $\frac{dw'}{dr'}$ is continuous to obtain a condition for the sonic velocity to obey,

$$2m v_*^3 = (\gamma - 1) r_* (f_e q_{e_*} \Lambda_{e_*} + f_\alpha q_{\alpha_*} \Lambda_{\alpha_*}) \tag{31}$$

We observe that Eq. (23) remains singular at the sonic radius, which can be corrected by evaluating $\frac{dw'}{dr'}$ at $r' = 1$ explicitly by l'Hospital's rule. We obtain

$$\frac{dw'}{dr'}(r' = 1) = \frac{2(3 - \gamma)}{\gamma + 1} + \frac{4}{\gamma + 1} \sqrt{\frac{(3-\gamma)^2}{2} - \frac{(\gamma+1)}{2} (F-1)} \tag{32}$$

$$\text{with } F = \frac{\lambda_*}{1 + f_r} + \frac{1}{\Lambda_{e_*}(1+f_r)} \frac{d\Lambda e}{dr} \quad (r = r_*) + \frac{\lambda_* \Lambda_{\alpha_*} f_r}{\Lambda_{e_*}(1+f_r)}$$

$$+ \frac{f_r}{\Lambda_{e_*}(1+f_r)} \frac{d\Lambda_\alpha}{dr} \quad (r = r_*)$$

$$\text{and} \quad f_r = \frac{f_\alpha q_{\alpha_*} \Lambda_{\alpha_*}}{f_e q_{e_*} \Lambda_{e_*}} .$$

The boundary conditions indicated by Eqs. (20) and (22) for the eigenvalue calculations are similarly reduced to

$$q'_e(\hat{r}) + q'_\alpha(\hat{r}) = 0 \tag{33}$$

$$\text{and} \quad w'(\hat{r}) = 0 \tag{34}$$

$$\text{with } \hat{r} = r_p/r_* \tag{35}$$

Equations (23) to (28), with boundary conditions at the pellet surface $r' = \hat{r}$ and at the sonic radius $r' = 1$, form a standard eigenvalue problem with the eigenvalue λ_* to be determined. We integrate Eqs. (23) to (28) by a Runge-Kutta numerical integration scheme to solve for the set of coupled differential equations. For only one ablating species, the numerical calculation needs only one initial input, the energy of the ablating particles at the sonic radius. Then the equations are integrated from $r' = 1$ to $r' < 1$ until a solution is located for a correct choice of λ_* that $q' = 0$ and $w' = 0$ at $r' = \hat{r}$. The boundary value $\hat{r}$ is also an initial unknown variable of problem that is uniquely determined when the eigenvalue solution is obtained. Then, we can proceed to find the plasma conditions far away from the pellet corresponding to this dynamic system. We integrate from the sonic radius to $r \to \infty$, i.e., when q' and E' converge to constant asymptotic values of $\hat{q}$ and $\hat{E}$ respectively. Hence the external plasma conditions are related by

$$q_\infty = \hat{q}\, q_* \tag{36}$$

$$E_\infty = \hat{E}\, E_* \tag{37}$$

For our electrons and alphas ablating system, we study the pellet ablation rate for the range $0 < n_\alpha/n_e \leq 0.1$. The alpha ablation enhancement will be formulated in the parameter n_α/n_e. For each run with a given n_α/n_e, we need to specify three parameters E_{e_*}, E_{α_*}, and q_{α_*}/q_{e_*} as initial input for the numerical integration as compared to only one independent variable for the electron ablation problem. We use an iterative scheme in order to have a self-consistent ablation cloud dynamic system with the external plasma conditions and reduce to one independent input variable in E_{e_*}. At the beginning of the integration, we guess the asymptotic values $\hat{E}_e$, $\hat{E}_\alpha$, and $\hat{q}_\alpha/\hat{q}_e$. We then obtain E_{e_∞} from $\hat{E}_e$, which enables us to find E_{α_∞} and $q_{\alpha_\infty}/q_{e_\infty}$. Finally, we determine E_{α_*} and q_{α_*}/q_{e_*} from $\hat{E}_\alpha$ and $\hat{q}_\alpha/\hat{a}_e$, respectively. We check the consistency of our initial guesses of the asymptotic values after an eigenvalue solution is obtained. The calculations are repeated until the guessed asymptotic values converge.

IV. Numerical Results

The calculations of pellet ablation with plasma electrons and fast alphas are computed for the ranges of $0 \lesssim T_e \leq 30$ keV and $0 \leq n_\alpha/n_e \leq 0.1$. The eigenvalue λ_* for a given plasma condition (T_e and n_α/n_e) is searched by repeating the numerical integration to satisfy the boundary conditions at the pellet surface. Once the correct eigenvalue is found, the cloud dynamics can be solved by the numerical integration, and the pellet ablation rate can be evaluated from the asymptotic values $\hat{r}$, $\hat{E}$, $\hat{q}$.

The pellet ablation rate G as appeared in Eqs. (13) and (15) can be formulated in terms of the numerically computed variables for the electrons and alphas ablation model. From Eq. (13) evaluated at the sonic radius, we obtain

$$G = 4\,\pi\,\rho_*\,V_*\,r_*^2 \tag{38}$$

in which ρ_* and V_* can be eliminated by substituting them with the relations in Eqs. (30) and (31). The unknown variables at the sonic radius is then

replaced by the asymptotic values through Eqs. (35) - (37). Hence, we find an expression of the ablation rate as

$$G = \frac{4\pi(\gamma-1)^{1/3}\, m^{2/3}\, r_p^{4/3}\, \lambda_*}{2^{1/3}\, \hat{r}^{4/3}\, \Lambda_{e*}} \left[\frac{n_{e\infty} V_{e\infty} E_{e\infty}}{4} \left(\frac{f_e \Lambda_{e*}}{\hat{q}_e} + \frac{R_\infty f_\alpha \Lambda_{\alpha*}}{\hat{q}_\alpha}\right)\right]^{1/3} \qquad (39)$$

where R_∞ is the ratio of the alpha and electron energy fluxes given by

$$R_\infty = \frac{n_{\alpha\infty}\, V_{\alpha\infty}\, E_{\alpha\infty}}{n_{e\infty}\, V_{e\infty}\, E_{e\infty}} \quad .$$

The contributions of the fast alphas can be basically visualized through Eq. (39). The last term of Eq. (39) shows explicitly the contribution of the alphas in depositing energy to heat the expanding cloud. This heating term is proportional to the flux attenuation cross section and the ratio R_∞. The other effect of alphas is to increase the thickness of the cloud required to shield the incident energy fluxes. This effect is reflected in the numerical solution of the term $\lambda_* r_* / \Lambda_{e*}$.

The pellet ablation rate may also be interpreted by the pellet surface regression speed $\dot{r}_p$, which is more convenient for computational purposes, as

$$\dot{r}_p = \frac{G}{4\pi \rho_s\, r_p^2} \qquad (40)$$

where ρ_s is the solid density of the pellet. We may rearrange Eq. (39) to separate the constants and independent variables with the eigenvalue solution results to obtain:

$$\dot{r}_p = 3.10 \times 10^{-18}\, \frac{M_o^{2/3}}{\rho_s}\, r_p^{-2/3}\, n_e^{1/3}\, T_e^{1/2}\, Z\left(T_e, \frac{n_\alpha}{n_e}\right) \qquad (41)$$

where we have used $\gamma = 7/5$ and M_o is the pellet molecular weight in amu. The function Z is calculated from numerical solutions which depend on initial inputs of T_e and $\frac{n_\alpha}{n_e}$, is given by

$$Z = \frac{\lambda_*}{\hat{r}^{4/3}} \left(\frac{f_e}{\hat{q}_e \Lambda_{e*}^2} + \frac{R_\infty f_\alpha \Lambda_{\alpha*}}{\hat{q}_\alpha \Lambda_{e*}^3} \right)^{1/3} \tag{42}$$

We now turn to the numerical solution of the pellet ablation eigenvalue problem. We examine, for example, the plasma conditions of $n_\alpha/n_e = 0.03$ and $E_{e*} = 30$ keV. Figure 1 shows the normalized density ρ/ρ_* and expansion kinetic energy w/w_* as a function of the normalized radius r/r_*. The density falls off rapidly as the molecules are evaporated from the pellet surface. The molecules pick up kinetic energy gradually in the expansion. In an equilibrium, these parameters have to satisfy the conservation of mass for a symmetric spherical expansion, i.e., $\rho v r^2$ is constant. It should be noted that the sonic radius is very small, less than the diameter of the pellet in this case.

In Fig. 2, the normalized electron and alpha energy fluxes are plotted with the normalized radius. We note that most of the energy fluxes are deposited within the sonic radius. The actual value of alpha energy flux is small compared to that of the electron energy flux, we find $q_{\alpha*}/q_{e*} \sim 0.15$. The electrons are able to penetrate into the pellet surface while the alphas are completely stopped in the shielding cloud before reaching the pellet.

The eigenvalue λ_* and the asymptotic values $\hat{q}_e$, $\hat{E}_e$, $\hat{q}_\alpha$ and $\hat{r}$ are shown in Figs. 3 and 4 as a function of T_e as illustrated by the case of $n_\alpha/n_e = 0.03$. The parameter $\hat{E}_\alpha$ is not shown here because it has the same value as $\hat{q}_\alpha$; this is because we ignore scattering for alphas so that the energy flux attenuation is only due to energy loss. Each value of λ_* on the curve is the unique eigenvalue for the corresponding plasma electron temperature, which then completely determines the cloud dynamics and the asymptotic parameters at that electron temperature. The parameter $\hat{r} = r_p/r_*$ is a measure of the magnitude of the sonic radius. We see that the sonic radius remains fairly constant over the range of electron temperature shown and has a minimum at about 11 keV. Similarly, $\hat{q}$ and $\hat{E}$ represent the effectiveness of shielding of the energy flux and energy up to the sonic radius. For high T_e, the alpha energy flux is attenuated more rapidly in the supersonic region; and vice-versa for low T_e. The electron energy attenuation in the supersonic region is small, therefore a larger fraction of electron energy flux loss is due to scattering losses.

V. Interpretation of Results and Scaling Law Derivation

We can now obtain a scaling law for the pellet radius regression rate by fitting the values of Z in Eq. (42) as a function of T_e for various fractions n_α/n_e, then substitute the results into Eq. (41). In addition, we can illustrate the enhancement of the pellet ablation rate from alphas by comparing the combined electron and alpha ablation rate to the electron ablation rate alone.

The electron ablation rate can be calculated by suppressing the alpha contribution ($n_\alpha/n_e = 0$ and $q_{\alpha*}/q_{e*} = 0$) in our set of equations, which is reduced to the results of Ref. 8. The ratio of the ablation rates is computed numerically and shown in Fig. 5 for the cases of n_α/n_e equals 0.01 and 0.05. We observe that for T_e approximately above 10 keV, the alphas provide a small and roughly constant enhancement. For T_e below 10 keV, the ablation enhancement is large with the alphas dominating at a larger n_α/n_e fraction and lower T_e. This is consistent with our assessment of the range of electrons and alphas in Section II. For our monoenergetic representation of electrons and alphas, the electrons have a longer penetration range than the alphas at T_e above 10 keV, and vice-versa. Hence at T_e above 10 keV, the shielding cloud thickness is basically determined by the incident electron flux which reaches the pellet surface. The alphas contribute mainly in the heating of the expanding cloud. As T_e varies from 10 to 30 keV, the electron energy flux scales as $T_e^{3/2}$ while the alpha energy flux remains roughly constant for a fixed ratio of n_α/n_e. As T_e increases, the alphas have less penetration resulting in relatively more energy depositing in heating the cloud around the sonic region. Recalling the heating term in Eq. (39), we see that R_∞ decreases and $\Lambda_{\alpha*}/\Lambda_{e*}\hat{q}_\alpha$ increases as T_e is raised, with the net result of slightly reducing the alpha ablation enhancement. The reduction of the alpha ablation enhancement is small because the ablation rate only varies to the 1/3 power of the heating term.

As a result, we may assume an average constant alpha enhancement over the range of 10 keV $\leq T_e \leq$ 30 keV. In Fig. 6, we plot the averaged alpha enhancement factor versus the alpha and electron density ratio. The enhancement varies linearly with the density ratio, having a slope of 5 for $n_\alpha/n_e \leq 3\%$ and 2.82 for $n_\alpha/n_e > 3\%$.

Now the scaling law for electron ablation alone from Ref. 8 is in the form of

$$\dot{r}_p = 1.72 \times 10^{-8} \, r_p^{-2/3} \, n_e^{1/3} \, T_e^{1.64} \tag{43}$$

To include the alpha effect, we can now modify the above scaling law for $10 \text{ keV} \leq T_e \leq 30 \text{ keV}$ to give

$$\dot{r}_p = 1.72 \times 10^{-8} \left(1 + C_\alpha \frac{n_\alpha}{n_e}\right) r_p^{-2/3} \, n_e^{1/3} \, T_e^{1.64} \tag{44}$$

where $C_\alpha = \begin{cases} 5.00 & \text{for } n_\alpha/n_e \leq 0.03 \\ 2.82 & \text{for } n_\alpha/n_e > 0.03 \end{cases}$

and the units for $\dot{r}_p$, r_p, n_e, and T_e are cm/sec, cm, cm^{-3}, and eV, respectively.

The alpha enhancement has a very sensitive dependence on the electron temperature and density ratio for $T_e < 10$ keV that makes a scaling law similar to Eq. (44) very difficult. However, since we know that alphas are dominant in this range, the magnitude of the combined electron and alpha ablation rate should not change much with T_e. Therefore, it is more convenient to examine the total ablation rate as a function of T_e. The electron temperature dependence of the ablation rate is in the function Z and explicitly in $T_e^{1/2}$. This dependence is plotted in Fig. 7. For $T_e > 10$ keV, we see the similarity with electron ablation in the T_e dependence ($T_e^{1/2} \, Z \sim T_e^{1.64}$). The ablation rate is greatly enhanced in the presence of the alphas for T_e below 10 keV, and is almost solely determined by the density ratio.

We could take an average value of $T_e^{1/2} \, Z$ for each n_α/n_e and construct a T_e independent ablation scaling law for this range of T_e. However, we take an alternative scheme which enables us to recover the electron ablation scaling law at $n_\alpha/n_e = 0$, and the scaling of Eq. (44) at $T_e = 10$ keV. The formalism should also reflect the strong dependence on n_α/n_e and lesser variation in T_e. We obtain an ablation scaling law by numerically fitting our results for $0 \leq T_e \leq 10$ keV in the form:

$$\dot{r}_p = 6.24 \times 10^{-2} \left(1 + C_\alpha \frac{n_\alpha}{n_e}\right) r_p^{-2/3} n_e^{1/3} \left(\frac{T_e}{10^4 \text{ eV}}\right)^{x_\alpha} \qquad (45)$$

with $x_\alpha = 1.64 \exp\left(-50 \frac{n_\alpha}{n_e}\right)$.

Equations (44) and (45) provide simple scaling laws for pellet ablation calculations to include the effect of fusion-born alpha particles in the ranges of $0 \leq n_\alpha/n_e \leq 0.1$ and $0 \leq T_e \leq 30$ keV. The expressions for the ablation rate are derived for a hydrogen pellet. We can see from Eq. (41) that the ablation rate is proportional to $M_o^{2/3}/\rho_s$, where M_o is the molecular mass number and ρ_s is the solid density of the pellet. Therefore, the ablation rate should be reduced by factors of 0.68 and 0.57 for deuterium and tritium pellets, respectively. We allow the parameter n_α/n_e to be an independent variable of the scaling laws instead of applying the classical slowing down value indicated by Eq. (6). This gives provision for alpha transport that may significantly alter the radial density profile from the birth profile.

The main uncertainty in our model is the monoenergetic representation of the slowing down alpha distribution using the average energy suggested in Ref. 16. This issue can only be resolved experimentally from alpha producing plasmas, which probably will not be operated in the near future. Because of this uncertainty, we have estimated the relative change of the pellet ablation rate due to the change of the mean alpha energy. We repeated the calculations for $n_\alpha/n_e = 0.05$ and fixed the mean alpha energy at 2.5 MeV (as opposed to the slowing down theory calculation that leads to $\langle E_\alpha \rangle \sim 1.7$ to 2.0 MeV). We have found that the pellet ablation rate will be increased by about 50% for $T_e <$ 10 keV and about 8% for $T_e >$ 10 keV. The relative increment of the ablation rate is obvious from the roles of the alphas in the two ranges of T_e.

VI. Application to the TIBER ETR

The scaling laws derived above are applied to TIBER,[19] a U.S. Engineering Test Reactor conceptual design. The plasma density and temperature profiles have the form of

$$x(r) = x_o \left(1 - \left(\frac{r}{a}\right)^2\right)^\alpha$$

where x_o is the peak axial value, a is the minor radius, and α is a profile adjusting exponent. For the TIBER steady-state mode operation, T_{eo} = 24.7 keV, α_T = 0.58, n_{eo} = 2.22 x 10^{14} cm^{-3}, α_n = 1.02, and a = 83.4 cm. The ratio n_α/n_e is taken from classical slowing down value given by Eq. (6) following the alpha birth profile.

For TIBER, we find alphas provide about 5% enhancement of the ablation rate. The injection velocities required for a/3 and a/2 penetration of a 10% inventory fuel pellet are 22.2 km/s and 52.4 km/s, respectively. The alpha effect in the pellet ablation is relatively small because an appreciable fraction of alphas is produced only at the high electron temperature regions where the ablation is dominated by the electrons. At lower electron temperatures where alpha ablation is significant, there is insufficient alpha production to create any drastic increase in the ablation rate. However, if large alpha orbit and transport effects are appropriately included, the alpha ablation enhancement might be expected to increase accordingly.

VII. Summary and Conclusions

We have studied the two plasma species, electrons and fusion-born alpha particles, which contribute to pellet ablation in a reactor-grade plasma. A neutral shielding transonic flow model is adapted and extended for our modeling of the ablation process. The electrons and alphas are represented by monoenergetic beams with appropriate mean energies. We have compared the penetration ranges of electrons and alphas and found that electrons with mean energy above about 10 keV have a larger range in the ablation cloud than that of fusion alphas with a characteristic mean slowing down energy. The ablation calculations are formulated as an eigenvalue problem with six coupled differential equations describing the shielding cloud dynamics and the degradation of the electron and alpha energies and energy fluxes. The equations are integrated numerically by a Runge-Kutta scheme with the boundary conditions at the pellet surface and the unperturbed plasma far away from the pellet. We have examined the solutions of the eigenvalue problem and the expanding cloud dynamics. The pellet ablation rate can be calculated from the numerical results. We have observed that the alphas provide a fairly constant enhancement of the ablation rate for electron temperatures approximately above 10 keV

due to the heating of the expanding cloud. At electron temperatures below 10 keV, the alphas have sufficient penetration relative to electrons to significantly affect the shielding cloud thickness, resulting in a dominant effect in the ablation rate. Two simple scaling laws have been formulated to include the alphas for the ablation rate calculations. The results are applied to the TIBER Engineering Test Reactor design and we find the alphas increase the ablation rate and hence the required injection velocity by about 5%. A larger enhancement of the ablation rate is expected if the alpha transport effects are included to allow higher alpha density fractions in the lower electron temperature regions. Future refinements of this modeling could include, for example, the effects of cold plasma shielding.[13]

REFERENCES

1. C.T. Chang, L.W. Jorgensen, P.N. Nielson, and L.L. Lengyel, "The Feasibility of Pellet Re-Fueling of a Fusion Reactor," Nucl. Fusion 20 859 (1980).
2. S.L. Milora, "Review of Pellet Fueling," J. Fusion Energy 1 15 (1981).
3. L. Spitzer, Jr., D.J. Grove, W.E. Johnson, L. Tonks, and W.R. Westendorp, "Problems of the Stellarator as a Useful Power Source," USAEC Report NYO 6047 (1954).
4. D.J. Rose, "On the Fusion Injection Problem," Tech. Div. Mem. No. 82, Culham (1968).
5. C.T. Chang, "The Magnetic Shielding Effect of a Re-Fueling Pellet," Nucl. Fusion 15 595 (1975).
6. S.L. Gralnick, "Solid Deuterium Evaporation in a Fusion Plasma," Nucl. Fusion 13 703 (1973).
7. P.B. Parks, R.J. Turnbull, and C.A. Foster, "A Model for the Ablation Rate of a Solid Hydrogen Pellet in a Plasma," Nucl. Fusion 17 539 (1977).
8. P.B. Parks and R.J. Turnbull, "Effect of Transonic Flow in the Ablation Cloud on the Lifetime of a Solid Hydrogen Pellet in a Plasma," Phys. Fluids 21 1735 (1978).

9. S.L. Milora and C.A. Foster, "A Revised Neutral Gas Shielding Model for Pellet-Plasma Interactions," IEEE Trans. Plasma Sci. 6 578 (1978).
10. L.L. Lengyel, "Pellet Ablation in Hot Plasmas and the Problem of Magnetic Shielding," Phys. Fluids 21 1945 (1978).
11. D.F. Vaslow, "Scaling Law For Ablation of a Hydrogen Pellet in a Plasma," IEEE Trans. Plasma Sci. P5-5 12 (1977).
12. M. Kaufmann, K. Lackner, L. Lengyel and W. Schneider, "Plasma Shielding of Hydrogen Pellets," Nucl. Fusion 26 171 (1986).
13. W.A. Houlberg, S.L. Milora, and S.E. Attenberger, "Neutral and Plasma Shielding Model for Pellet Ablation," submitted to Nucl. Fusion.
14. S.L. Milora, "New Algorithm for Computing the Ablation of Hydrogenic Pellets in Hot Plasma," Oak Ridge National Laboratory Report ORNL/TM-8616 (1986).
15. Y. Nakamura, H Nishihara, and M. Wakatani, "An Analysis of the Ablation Rate for Solid Pellets Injected into Neutral Beam Heated Toroidal Plasmas", Nucl. Fusion 26 907 (1986).
16. S.L. Milora, et al., "Results of Hydrogen Pellet Injection into ISX-B," Nucl. Fusion 20 1491 (1980).
17. W.T. Miles, R. Thompson, and A.E.S. Green, "Electron-Impact Cross Sections and Energy Deposition in Molecular Hydrogen", J. Appl. Phys. 43 678 (1972).
18. L.J. Perkins and M.C. Scott, "The Application of Pulse Shape Discrimination in NE 213 to Neutron Spectrometry," Nucl. Instruments and Methods 166 451 (1979).
19. J.D. Lee, ed., "TIBER II Engineering Test Reactor--Final Report," Lawrence Livermore National Laboratory, UCID-21150, (to be published 1987).

ACKNOWLEDGMENTS

One of us, (SKH), acknowledges support of the U.S. Department of Energy Fusion Energy Postdoctoral Research Program administered by Oak Ridge Associated Universities. We are grateful to Ms. D. Jalanivich for the careful preparation of this manuscript.

FIGURE CAPTIONS

Fig. 1. Normalized shielding cloud kinetic energy w/w_* and density ρ/ρ_* versus the normalized radial position r/r_*. The subscript * denotes variables at the sonic radius.

Fig. 2. Normalized electron energy flux q_e/q_{e*} and alpha energy flux $q_\alpha/q_{\alpha*}$ versus the normalized radial position r/r_*.

Fig. 3. The eigenvalue λ_* and the asymptotic normalized pellet radius $\hat{r}$ as a function of the electron temperature.

Fig. 4. The asymptotic normalized electron energy $\hat{E}_e$, electron energy flux $\hat{q}_e$, and alpha energy flux $\hat{q}_\alpha$ as a function of the electron temperature.

Fig. 5. Ratio of the pellet ablation rate due to electrons with alphas to that of electrons, for two alpha density fractions, versus the electron temperature.

Fig. 6. Ratio of the pellet ablation rate due to electrons with alphas to that of electrons as a function of the alpha density fraction.

Fig. 7. The electron temperature dependence of the ablation rate in $T_e^{1/2} Z$ versus the electron temperature.

(dj711388/skhp)

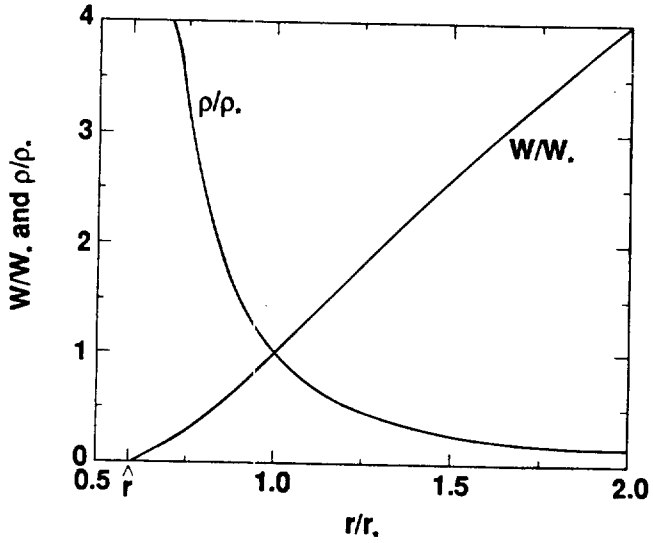

Figure 1

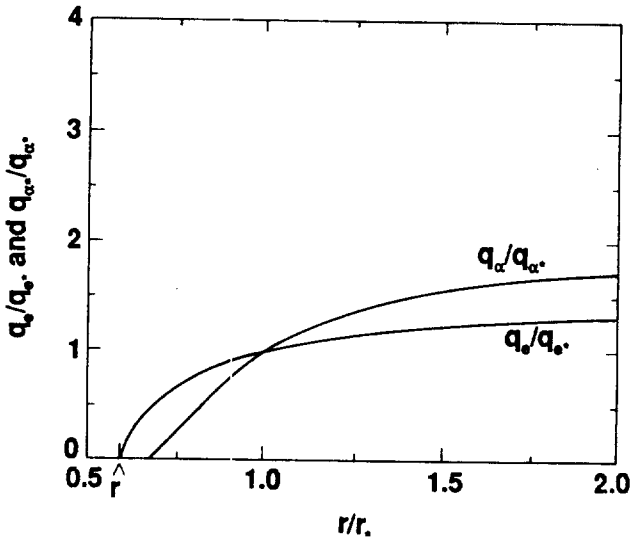

Figure 2

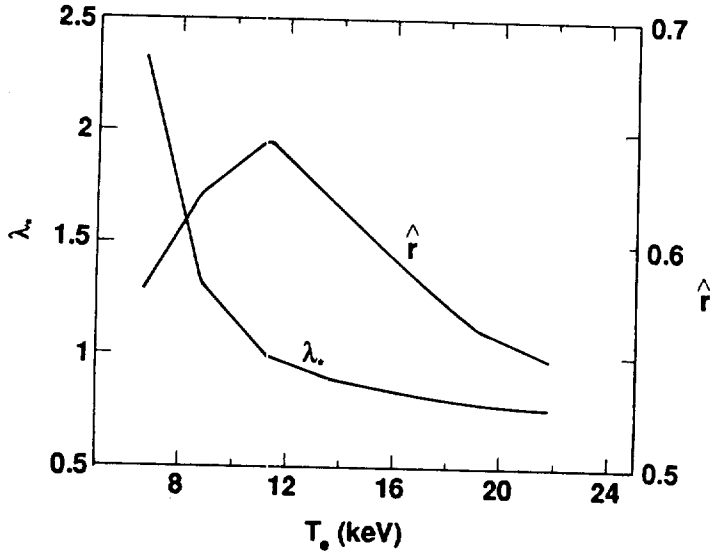

Figure 3

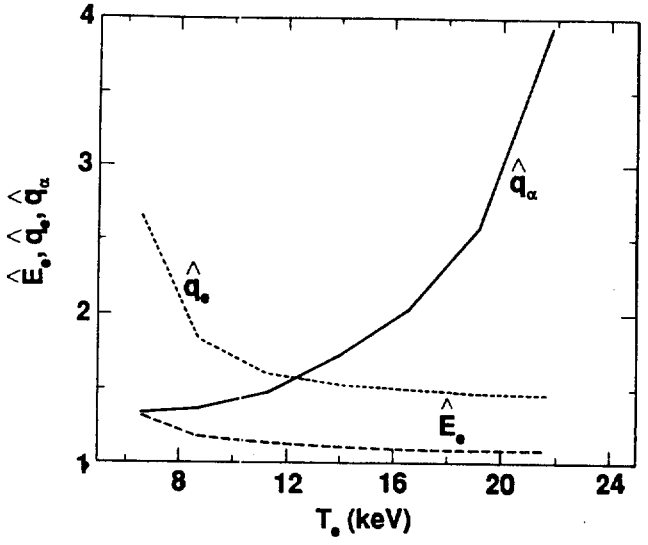
4
3
2
1
8
12
16
20
24
T_e (keV)
$\hat{E}_e, \hat{q}_e, \hat{q}_\alpha$
$\hat{q}_\alpha$
$\hat{q}_e$
$\hat{E}_e$

Figure 4

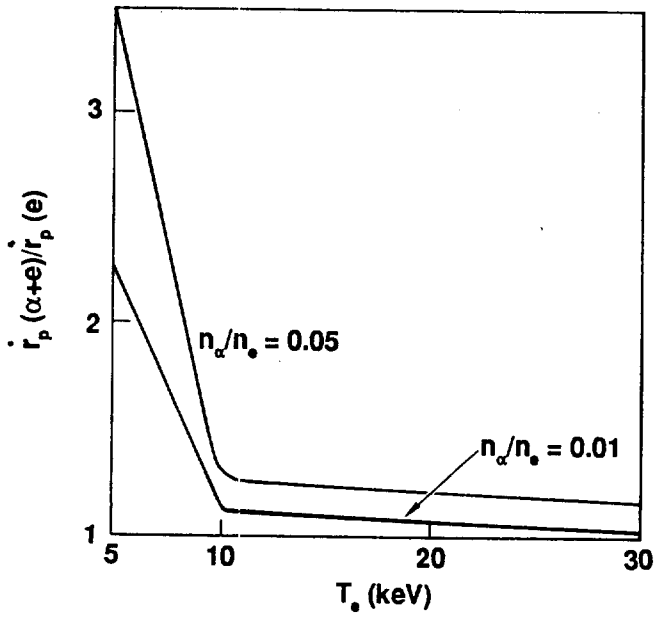
3
2
1
5
10
20
30
$\dot{r}_p(\alpha+e)/\dot{r}_p(e)$
$n_\alpha/n_e = 0.05$
$n_\alpha/n_e = 0.01$
T_e (keV)

Figure 5

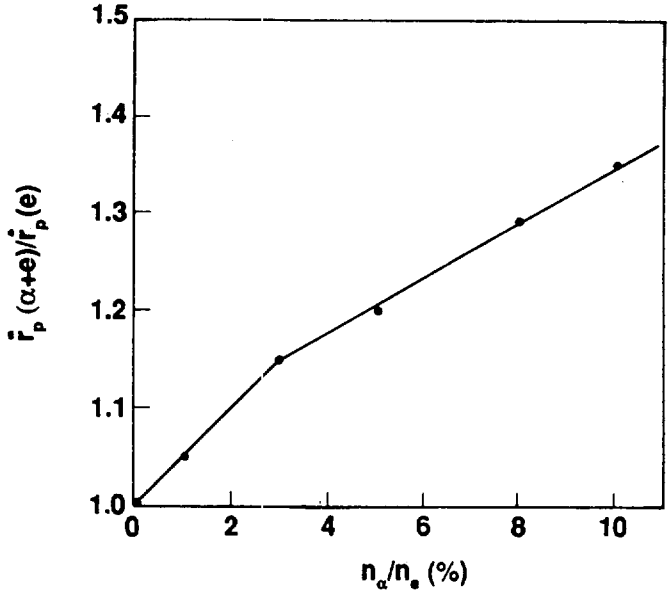

Figure 6

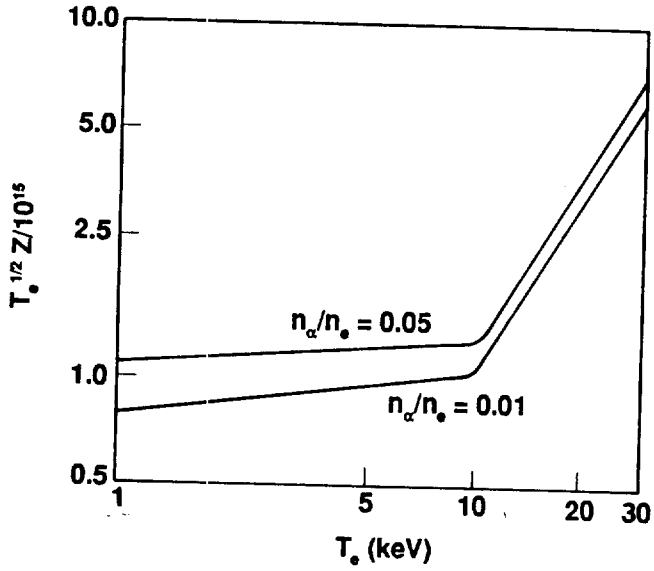
10.0
5.0
2.5
1.0
0.5
$T_e^{1/2}$ Z/10^{15}
n_α/n_e = 0.05
n_α/n_e = 0.01
1
5
10
20
30
T_e (keV)

Figure 7